A&A 418, 41–52 (2004)
DOI: 10.1051/0004-6361:20034012

Astronomy & Astrophysics

Photometric structure of the peculiar galaxy ESO 235-G58

E. Iodice[1], M. Arnaboldi[1,2], L. S. Sparke[3], R. Buta[4], K. C. Freeman[5], and M. Capaccioli[1,6]

[1] INAF-Osservatorio Astronomico di Capodimonte (OAC), via Moiariello 16, 80131 Napoli, Italy
[2] INAF-Osservatorio Astronomico di Torino, Strada Osservatorio 20, 10025 Pino Torinese, Italy
[3] Dept. of Astronomy, University of Wisconsin, 475 N. Charter St., Madison, WI, USA
[4] University of Alabama, Department of Physics & Astronomy, Box 870324, Tuscaloosa, Alabama 35487, USA
[5] RSAA, Mt. Stromlo Observatory, Canberra, Cotter Road, Weston ACT 2611, Australia
[6] Dept. of Physical Sciences, University "Federico II", Naples, Italy

Received 26 June 2003 / Accepted 20 January 2004

Abstract. We present the near-infrared and optical properties of the peculiar galaxy ESO 235-G58, which resembles a late-type ringed barred spiral seen close to face-on. However, the apparent bar of ESO 235-G58 is in reality an edge-on disk galaxy of relatively low luminosity. We have analyzed the light and color distributions of ESO 235-G58 in the NIR and optical bands and compared them with the typical properties observed for other morphological galaxy types, including polar ring galaxies. Similar properties are observed for ESO 235-G58, polar ring galaxies, and spiral galaxies, which leads us to conclude that this peculiar system is a *polar-ring-related* galaxy, characterized by a low inclined ring/disk structure, as pointed out by Buta & Crocker in an earlier study, rather than a barred galaxy.

Key words. galaxies: peculiar – galaxies: individual: ESO 235-G58 – galaxies: photometry – galaxies: evolution

1. Introduction

The southern galaxy ESO 235-G58 is classified in RC3 (de Vaucouleurs et al. 1991) as an SB(rs)d spiral based on its appearance on the ESO/SRC-J Southern Sky Survey. It is characterized by a quite elongated bar-like structure, for which the total extension is ∼40″ and the position angle (PA) of its major axis is 106°. This apparent bar is encircled by a weak inner pseudo-ring and two faint outer arms, which reach a distance of about 1′ from the center (Fig. 1). Using $H_0 = 70\,\mathrm{km\,s^{-1}\,Mpc^{-1}}$, the galaxy has a distance of about 67 Mpc. In this early classification the galaxy disk is seen nearly face-on, with a pseudo-ring at about 1′ from the center, encircling an inner bar.

Closer inspection of ESO 235-G58 (Buta 1995), in the *Catalogue of Southern Ringed Galaxies*, led to the suspicion that the apparent central bar is in reality an edge-on disk. With new optical data, Buta & Crocker (1993) showed that ESO 235-G58 is probably not a ringed barred spiral of late Hubble type, because the central elongated structure shows a nearly linear dust lane which splits the nuclear region in a way which is typical of edge-on disks (see Fig. 1). This implies that the equatorial plane of the central structure is at a different angle to the line of sight than the outer ring. The analysis of these optical data (Buta & Crocker 1993) suggested that ESO 235-G58 is composed of a low luminosity edge-on disk, with an equatorial dust-lane, and an outer ring/spiral at very large radii, seen at a lower inclination. Therefore, ESO 235-G58 may be a good candidate for Polar-Ring-related objects. Polar Ring galaxies (PRGs) are usually recognized because the two components (the host galaxy and ring) are nearly edge-on (Whitmore et al. 1990). It is more difficult to recognize cases where the inner component is edge-on, while the ring is more face-on: cases like that must exist and ESO235-G58 may be such kind of an object.

The main goal of the present work is to provide accurate optical and near-infrared (NIR) photometry of ESO 235-G58, and to compare the main properties of this galaxy with those typical of other morphological galaxy types, including PRGs. NIR photometry is necessary to minimize the dust absorption which strongly affects the starlight distribution in the central galaxy. In addition, the study of optical and NIR integrated colors will provide information about the age and metallicity of the dominant stellar population in the different components of the system. In this paper we present new NIR observations, obtained for ESO 235-G58 in J, H and Kn bands, and have applied the same procedures adopted to study PRGs by Iodice et al. (2002a,b,c). As shown by Iodice and collaborators, this kind of analysis allows us to obtain quantitative morphology of the main components in ESO 235-G58, in order to rigorously classify this object, and gain insight on its star formation history.

Observations and data reduction are presented in Sect. 2; the morphology, light and color distribution of the two components (host galaxy and ring) are discussed in Sects. 3 and 4. In Sect. 5 we describe the dust properties and how they

Send offprint requests to: E. Iodice, e-mail: iodice@na.astro.it

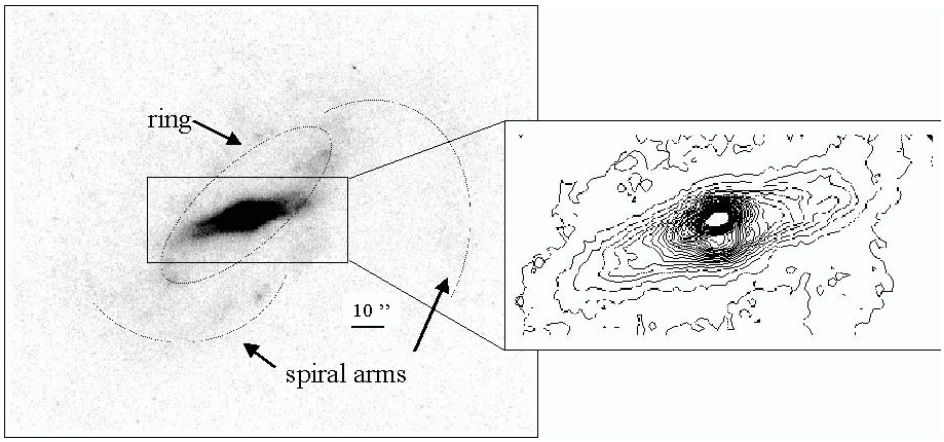

Fig. 1. *Left panel*: *B*-band image, by Buta & Crocker (1993), of the peculiar galaxy ESO 235-G58. *Right panel*: contour plot of the inner regions of ESO 235-G58, strongly perturbed by a dust lane which splits the galaxy along the major axis. North is at the top and East is to the left. Units are intensity.

Table 1. NIR log of observations for ESO 235-G58.

Filter	Tot. int. (s)	*FWHM* (arcsec)	Date
J	1200	1.6	19/08/1995
H	1200	1.5	19/08/1995
H	600	1.6	20/08/1995
*K*n	2400	1.5	18/08/1995
*K*n	600	1.4	20/08/1995

compare with the typical properties in other galaxies and the Milky Way. In Sect. 6 the integrated colors derived for the central galaxy and ring are presented, and in Sect. 7 we give an age estimate of the two components. The two-dimensional model of the central galaxy light distribution is discussed in Sect. 8, and in Sect. 9 we discuss the properties of the ring light distribution. A summary of the main results and conclusions is presented in Sect. 10.

2. Observations

ESO 235-G58 is a member of a selected sample of peculiar galaxies observed in the NIR *J*, *H* and *K*n[1] bands with the CASPIR infrared camera (McGregor 1994), attached to the Mt. Stromlo and Siding Spring Observatory 2.3 m telescope. The pixel scale is $0.5''$ pixel^{-1} and the field of view is $2.0' \times 2.0'$. A detailed description of the data reduction is given by Iodice et al. (2002b). The observing log for these data is summarized in Table 1.

The optical data were obtained by D. A. Crocker and L. V. Jones in 1992 with a TEK 1024 CCD array (with a pixel scale of $0.43''$ pixel^{-1}) attached to the 1.5 m telescope of Cerro Tololo Inter-American Observatory. The images were acquired in the Johnson *BV* and Cousin *I* filters, with total exposures of 1500 s in *B*, 600 s in *V* and 300 s in *I*. The reduction and analysis of these data were published by Buta & Crocker (1993). The *B* band and *H* band images are shown in Figs. 1 and 2 respectively.

[1] The central wavelength for *K*n filter is 2.165 μm.

3. Morphology in the NIR and optical bands

The *H* band image of ESO 235-G58 is shown in Fig. 2. The appearance of the galaxy in this band is remarkably different from what is observed in the *B* band (Fig. 1). The NIR morphology of ESO 235-G58 resembles that of an early-type, edge-on disk galaxy, similar to an Sa, while the ring and spiral arms, observed in the optical images, are not detected. The only NIR flux associated with this component is an asymmetric elongation, in the NW direction, of the central Sa disk (Fig. 2). This structure may be debris in the apparent ring feature, which, on the other hand, is evident in the *B* (Fig. 1) and *V* bands (see Buta & Crocker 1993). This indicates that the ring structure is much bluer than the central object.

The absence of squared-off ends, typical of bars in early-type spirals (Athanassoula et al. 1990; Jungwiert et al. 1997; Erwin & Sparke 2003), in the *H* band isophotes (see Fig. 2, right panels), make this object more similar to an edge-on disk galaxy than to a bar. This is further confirmed by the shape of the ellipticity and position angle profiles (shown in Fig. 2, bottom-left panel), derived by fitting ellipses[2] to isophotes of the *H* band image: the ellipticity profile suggests the existence of a round central component and an outer, more extended, flattened structure. The position angle is almost constant except for a variation of about four degrees in the range $16'' \leq R \leq 20''$. The ellipticity and PA profiles are quite irregular in the innermost regions ($R \leq 3''$): the first maximum value in the ellipticity corresponds to a minimum in the PA, at about $1''$ from the center. These variations could be caused by uncertainties in the fitting algorithm, induced by the few adopted points, as it is also suggested by the very regular aspect of the the inner isophotes, relative to this region (see Fig. 2, bottom-right panel). The ellipticity and PA profiles for ESO 235-G58 are quite different from those typically observed for barred galaxies, where the bar isophotes are very nearly circular in the innermost parts (it varies from 0.7 to 0.9) and gradually become more elongated with increasing radius (Athanassoula et al. 1990;

[2] We have used the IRAF task ELLIPSE to derive the ellipticity and PA profiles.

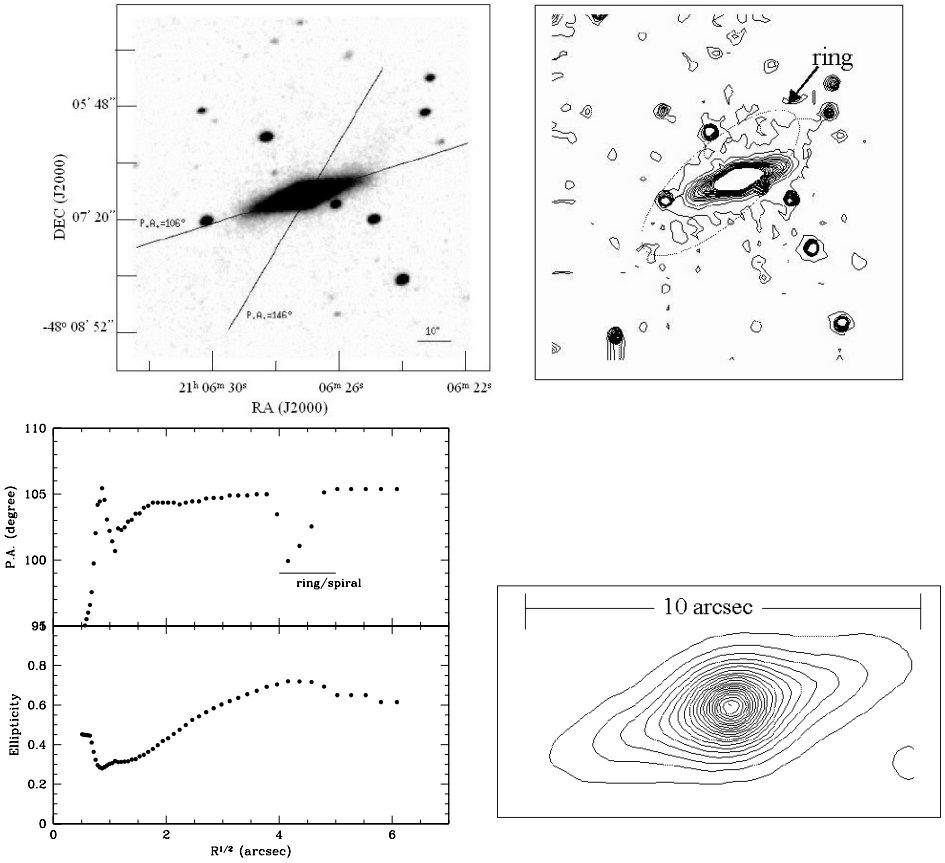

Fig. 2. *Top-left panel*: *H*-band image of ESO 235-G58; *top-right panel*: contour plot, with linear spacing, from the intensity level corresponding to 16.25 mag/arcsec^2 to background level. The lines at PA = 106° and PA = 146° show apparent major axes of the central galaxy and the outer ring respectively. The image size is $2' \times 2'$. North is at the top and East is to the left. In the bottom-left panel are shown the ellipticity and PA profiles along the major axis of the galaxy. In the bottom-right panel is shown the contour plot, with a linear spacing, of the inner regions ($R < 5''$) of the central galaxy, the last isophote corresponds to 16.45 mag/arcsec^2.

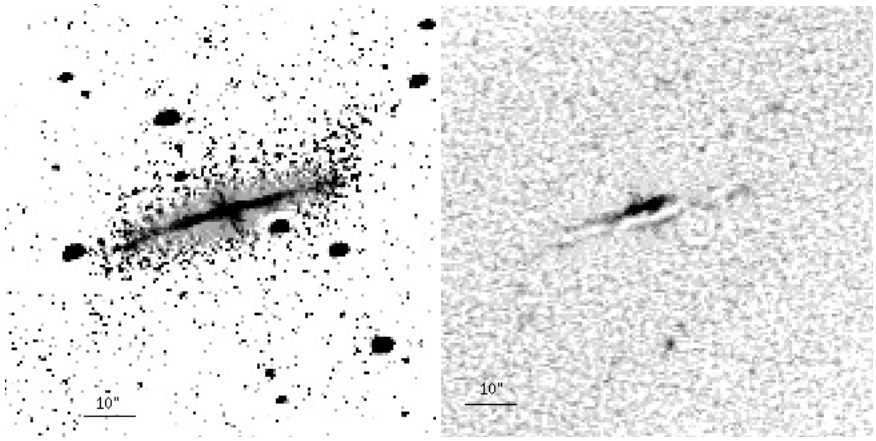

Fig. 3. High frequency residual image for ESO 235-G58 in the *H*-band (*left panel*) and in the *B* band (*right panel*). In the *B*-band image the foreground stars were masked. The darker regions are characterized by a value greater than 1, and lighter regions by a value less than 1. North is at the top and East is to the left.

Jungwiert et al. 1997); at the same time, a twisting is observed in the PA profile (Wozniak et al. 1995; Erwin & Sparke 2003). In the case of ESO 235-G58, the twisting observed in the PA profile, in the range $16'' \leq R \leq 20''$ (Fig. 2), is due to the projection of the ring light on to the central galaxy. The absence of a local maximum in the ellipticity profile in this range suggest that there is no additional component, like a bar, present. On the other hand, the ellipticity and PA profiles for ESO 235-G58 are very similar to the typical ellipticity and PA profiles observed for edge-on non-barred disk galaxies (S0s and spirals), where an almost round bulge and a prominent disk are present (Michard 1984; Scorza & Bender 1995).

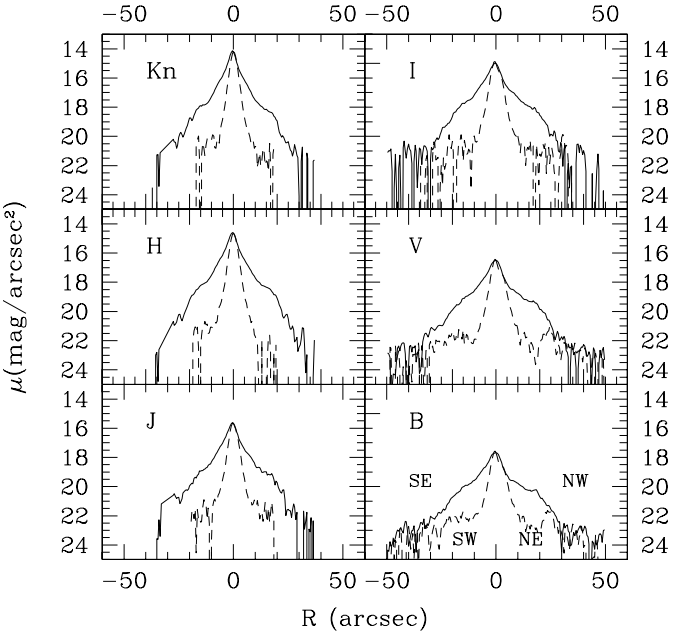

Fig. 4. NIR (*left panels*) and optical (*right profiles*) surface brightness profiles along the major, PA = 106°, (continuous line) and minor axis (dashed line) of the central galaxy.

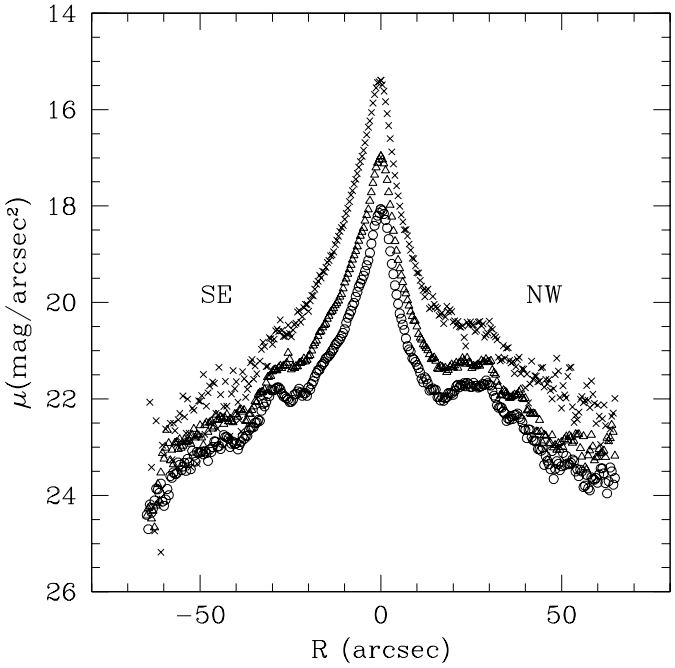

Fig. 5. Surface brightness profiles along the ring major axis, PA = 146°, in *B* (open circles), *V* (open triangles) and *I* bands (crosses).

The NIR unsharp masked images[3] (see Fig. 3 for *B* and *H* band) confirm that the central component in ESO 235-G58 is an edge-on disk galaxy: in the NIR unsharp masked images, a luminous nearly edge-on structure is clearly identified, along the major axis of the galaxy, (see left panel of Fig. 3 for the *H* band); this feature is then seen in absorption in the optical images (see right panel of Fig. 3 for the *B* band). It confirms that the disk is not completely edge-on because the dust lane does not split the bulge into two equal halves. Furthermore, a "filamentary" structure is visible in the *H* band, perpendicular to the disk and aligned with the apparent minor axis of the galaxy, extending approximately 10″. A similar feature was also observed in the polar ring galaxy ESO 603-G21 (Iodice et al. 2002b; Reshetnikov et al. 2002; Arnaboldi et al. 1995), where rotation was detected along a axis coincident with this filament, suggesting that it is a small edge-on disk. In the case of ESO 235-G58 we lack any kinematical data, thus no conclusions can be reached on the nature of this structure perpendicular to the main disk.

4. Photometry: Light and color distribution

The surface brightness profiles were derived along the major (PA = 106°) and minor axis of the central galaxy, in the NIR and optical bands, and they are shown in Fig. 4. The dust lane perturbs the optical minor axis profiles, making them slightly asymmetric. The *H* and *K*n band light profiles, in contrast, are not strongly influenced by the dust absorption. The analysis of the NIR light profiles, along the minor axis, shows that the bulge component extends out to 10″, at most; at large distances from the center, the additional light along this axis is related to the ring, which is brighter in the *B* and *V* bands.

From *B* to *J* bands, the light distribution along the NW direction, in the radial interval $5'' < R < 20''$, is more luminous than the corresponding regions along the SE direction: this excess is more likely related to the NW regions of the ring, identified also in the NIR bands as a bright elongation of the central galaxy disk in this direction (Sect. 3 and Fig. 2). The change in slope, observed at $R \sim 20''$ from the center, in both directions and in all bands, can not be caused by dust absorption alone, because it is clearly detected also in *H* and *K*n bands, where this perturbation is reduced to a minimum. This feature in the light profiles is observed in the same range of radii where the twisting of the PA profile is also detected (Fig. 2): they are consistent with the interpretation of ring light superposed to the galaxy light along the line of sight.

The surface brightness profiles for the ring structure, shown in Fig. 5, are obtained in the optical bands only, since this component is almost undetectable in the NIR bands, as described in Sect. 3. In order to cover the whole ring extension, including the spiral arms, the surface brightness profiles for this component are the results of an average of 40 profiles extracted in a cone, centered on the host galaxy and 10 degrees wide from the position angle of the ring major axis (PA = 146°, by Buta & Crocker 1993). On average, the ring light distribution seems to have an exponential profile; the several bumps, which strongly perturb the *B* and *V* profiles, are caused by star forming regions and dust in the ring structure (Fig. 1).

[3] The un-sharp masked images are obtained as ratios between the co-added galaxy frame and its median filtered image, which is the result of a median filtered image, computed with the FMEDIAN package in IRAF, where each original pixel value is replaced with the median value in a sliding rectangular window. After several tests, a window size of 7×7 pixels was chosen because it provides the optimum enhancement of the galaxy inner structures.

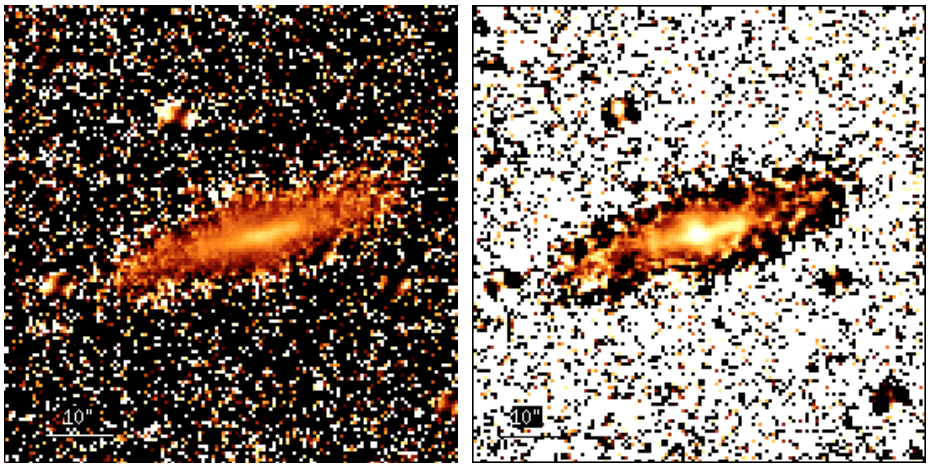

Fig. 6. $J - H$ (*left panel*) and $H - K$ (*right panel*) color map for ESO 235-G58. Darker regions correspond to bluer colors and lighter regions correspond to redder colors. North is at the top and East is to the left.

The $J - H$, $H - K$ color maps (Fig. 6) show that the nuclear regions of the galaxy, inside 10″ from the center, are redder than the outer ones: they correspond to the bulge component, whose extension has been previously estimated to be about 10″. The $B - K$ color map (Fig. 7) shows even more details of the structure of ESO 235-G58: the very red bulge is again seen, and the dust lane along the central object major axis is much redder than its surroundings. The very blue regions, all around the central galaxy, correspond to the ring structures, which appear more face-on with respect to the central object.

5. Dust properties

The central galaxy of ESO 235-G58 is characterized by a relatively high degree of symmetry and a high inclination: these properties make this object suitable for the study of the dust lane, which runs parallel to the major axis out to 17″ from the center of the galaxy (see Fig. 1). In order to estimate the extinction law in the dust lane, we adopted the same analysis used by Knapen and collaborators (Knapen et al. 1991) for the Sombrero galaxy (NGC 4594): in each band, we compare the surface brightness distribution of regions perpendicular to the dust lane, i.e. along the minor axis, which are at the same distance from the galaxy center. We then subtracted the unobscured part of the profile, i.e. the northern side, from its obscured counterpart, the southern side, in order to obtain the *absorption profile* defined by

$$A_\lambda(R) = -2.5 \log \frac{I_{\rm obs}(\lambda)}{I_{\rm true}(\lambda)}$$

where $I_{\rm obs}$ is the observed intensity at a given point in the dust lane and $I_{\rm true}$ is the intensity relative to the starlight with no dust obscuration. For this analysis, the exact center of the galaxy is determined from the K band image. The minor axis profile relative to the inner regions of the galaxy are shown in the left panel of Fig. 8: the dust absorption strongly perturbs the B band profile from the center to about 4″ radius on the SW side, while this effect is almost absent in the K band profile. The absorption profiles relative to each band are plotted in the middle panel of Fig. 8: the dust absorption is significant in the J band also, and becomes weaker in the H band. The absorption profile in the K band shows that there is no absorption caused by the dust lane in this region, but on the contrary it suggests that the SW side of the profile is brighter (about 0.4 mag) than the correspondent NE side. This is probably due to the twisting of the isophotes observed from the center to about 4″ (see Fig. 2) and "hidden" by the dust absorption in the other bands.

Table 2. Extinction ratios A_λ/A_V for the dust lane in ESO 235-G58, for the Sombrero galaxy (NGC 4594), for the polar ring galaxy NGC 4650A and for our Galaxy, in several bands.

Band	ESO 235-G58	NGC 4594	NGC 4650A	Our Galaxy
A_B/A_V	1.13 ± 0.04	1.20	1.11 ± 0.01	1.324
A_V/A_V	1.00	1.00	1.00	1.00
A_I/A_V	0.67 ± 0.06	0.52	0.83 ± 0.01	0.482
A_J/A_V	0.37 ± 0.11	0.31	0.31 ± 0.03	0.282
A_H/A_V	0.15 ± 0.09	0.19	0.20 ± 0.03	0.175
A_{K_n}/A_V	0.10 ± 0.06	0.09	0.14 ± 0.03	0.112

By using standard linear regression, we have obtained the values of the ratio A_λ/A_V presented in Table 2. These values are compared with those typical for our Galaxy (Rieke & Lebofsky 1985), for the Sombrero galaxy (Knapen et al. 1991) and for the polar ring galaxy NGC 4650A (Iodice et al. 2002a), for which we have derived the absorption coefficient profiles[4] shown in Fig. 8 (right panel). Taking into account the errors, the values of A_λ/A_V for ESO 235-G58 are consistent with those derived for the Sombrero galaxy and for NGC 4650A and for those relative to our Galaxy only in the near-IR, JHK bands. Major differences are observed between the A_λ/A_V for our Galaxy and those for the other three galaxies in the optical bands. As suggested by Knapen et al. (1991), such differences do not necessarily imply that the properties of the dust in our Galaxy are different from the other galaxies. Some fraction of the light in the dust lane does not originate behind the dust. In the simple

[4] We have compared the surface brightness profiles along the major axis of the host galaxy, where the dust in the polar ring obscures the SW regions (see Iodice et al. 2002a for details).

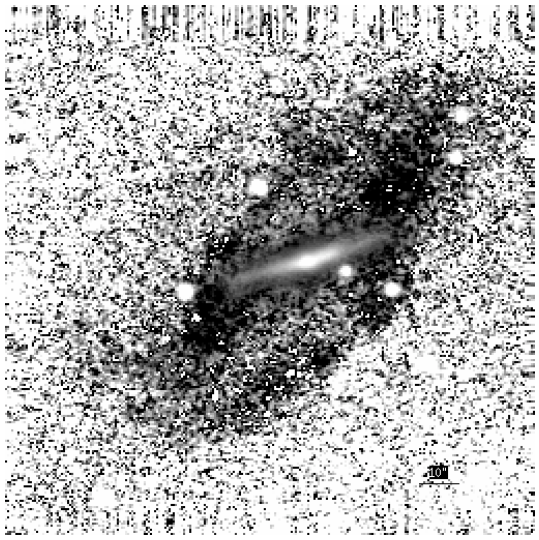

Fig. 7. $B-K$ color map for ESO 235-G58. Darker regions correspond to bluer colors and lighter regions correspond to redder colors. North is at the top and East is to the left.

models developed to describe this phenomenon (Walterbos & Kennicutt 1988) the absorption profile A_λ is also a function of the optical depth of the dust, which becomes progressively smaller toward longer wavelengths, implying an even smaller difference between the A_λ/A_V ratio for our Galaxy and for other galaxies.

6. Integrated magnitudes and colors

We wish to analyze the integrated colors derived for the main components (the central galaxy and ring) in ESO 235-G58, in order to compare them with those of standard morphological galaxy types. To this aim, the integrated magnitudes are computed in several areas which cover the two components and are selected differently in the optical compared to the NIR bands, because of the different morphologies in these bands (Sect. 3). A detailed discussion about the photometric error estimate, which takes into account both photon statistics and background fluctuations, was presented by Iodice et al. (2002b). In the optical bands they are about 3%, whereas in the NIR they are about 10%. The integrated magnitudes and colors derived in each area are then corrected for the galactic extinction within the Milky Way, by using the values for the absorption coefficient in the B band (A_B) and the color excess $E(B-V)$ derived from Schlegel et al. (1998). The absorption coefficients A_λ are derived for each band, by adopting $R_V = A_V/E(B-V) = 3.1$ from Cardelli et al. (1989).

6.1. Optical colors

In the B, V, and I bands, the areas where the integrated magnitudes are computed are selected as follows: one is coincident with the central galaxy, and two areas are for the ring structure, along the SE and NW directions (see Fig. 9). The polygons are determined in the B band, where the ring component is more luminous and extended, and they are used for the V and I images, previously registered to the B image. The integrated magnitudes and colors, derived for each area, are listed in Table 3. The $B-V$ vs. $V-I$ colors for the central galaxy and ring (Fig. 10) are compared with those of (1) standard early-type galaxies (Michard & Poulain 2000); (2) spiral galaxies (de Jong & van der Kruit 1994); (3) dwarf galaxies (Makarova 1999); (4) LSB galaxies (O'Neil et al. 1997; Bell et al. 2000), and (5) barred galaxies with outer rings and pseudo-rings (Buta & Crocker 1992). The colors of the central galaxy (which are redder[5] than those derived by Buta & Crocker 1993), taking into account the dust reddening, are within the range of colors for spiral and LSB galaxies.

Table 3. Integrated magnitudes and colors, in the optical bands, for the central galaxy and ring in ESO 235-G58.

Component	m_B	M_B	$B-V$	$V-I$
GALAXY	16.27	–17.6	0.98	1.37
RING (NW)	16.73	–17.2	0.32	0.81
RING (SE)	16.93	–17.0	0.39	0.51

The outer ring is much bluer than the central galaxy and the colors we find are consistent with the values derived by Buta & Crocker (1993). The optical colors of this component are similar to those of dwarf galaxies and the polar structure in the polar ring galaxy NGC 4650A (Iodice et al. 2002a), as shown in Fig. 10. The strong color gradient between the central galaxy and ring cannot be the effect of dust reddening only, since the reddening vector cannot account for the whole color difference. Therefore it implies a difference in stellar populations.

6.2. NIR colors

The study of the colors in the NIR concerns mainly the central galaxy, since the ring is hardly detected in these bands (see Sect. 3) and it is quite difficult to define any areas where magnitudes and colors can be reliably estimated. Five polygons[6], with the same center and larger areas, were defined starting from the galaxy contour in the Kn band. The largest polygon is determined from the outer isophote in the Kn band associated with the galaxy (Fig. 11). The integrated magnitudes and colors for the ring component were estimated from the difference between fluxes in the last two polygons. This choice is suggested by the excess blue light around the central galaxy in the NIR color maps (Fig. 6). The five polygons are used both for J and H bands and for the optical bands, after the images were registered and scaled to the Kn image. The integrated magnitudes and colors, corresponding to each area, are listed in Table 4. Figure 12 plots the $J-H$ vs. $H-K$ (left panel) and $B-V$ vs. $V-I$ (right panel) color diagrams. In both the NIR and in the optical, colors become bluer as area increases. In both color diagrams, on average, the central galaxy has colors very similar to those of spiral galaxies; the nuclear region of this component is characterized by the reddest colors.

[5] This is probably due to a different area chosen in the present work to estimate colors.

[6] These polygons are different from those defined for the optical images, described in Sect. 6.1.

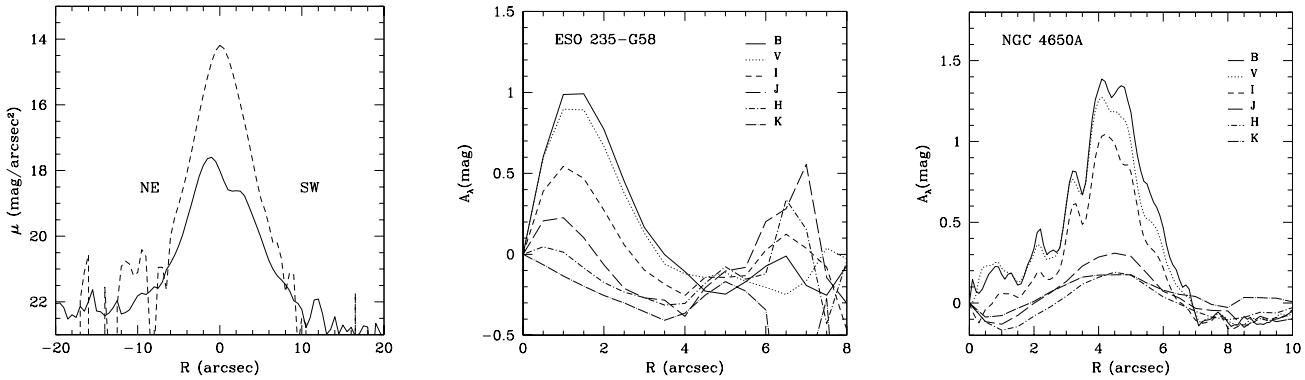

Fig. 8. *Left panel*: surface brightness profiles along the minor axis of the inner regions of ESO 235-G58 in B (continuous line) and in K band (dashed line). *Middle panel*: the extinction profile A_λ observed for the dust lane in ESO 235-G58, in the B, V, I, J, H and K bands. *Left panel*: the extinction profile A_λ observed for the dust lane in the polar ring galaxy NGC 4650A.

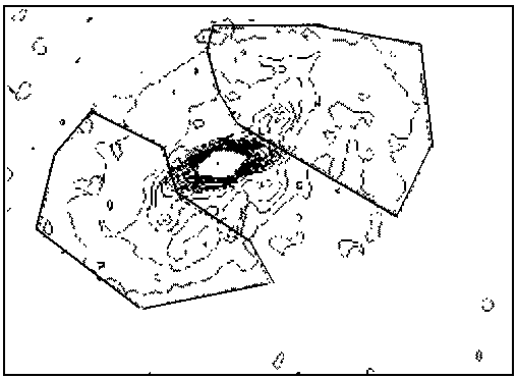

Fig. 9. ESO 235-G58 contour plot in B band (continuous line) plus the 3 polygons limiting the different areas where the integrated magnitudes are computed. The polygons enclosing the central galaxy (not clearly visible on the figure) is almost coincident with an ellipse whose major axis is about 20″. North is at the top and East is to the left.

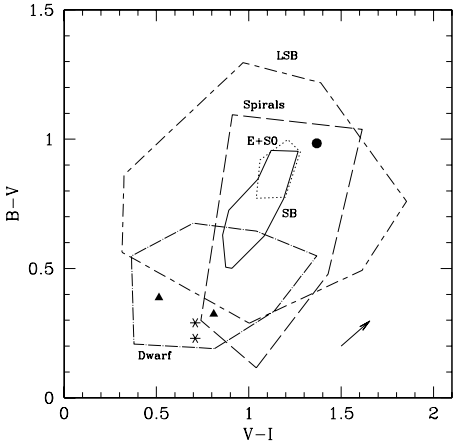

Fig. 10. $B-V$ vs. $V-I$ color diagram for the central galaxy (filled circle) and ring (filled triangles) in ESO 235-G58. Asterisks are the optical colors for the polar structure in NGC 4650A. The dotted contour limits the region where the integrated colors of Es and S0s are found; the long-dashed contour limits the integrated colors of spirals; the dashed-dotted contour identifies the integrated colors of the dwarf galaxies, the long dashed – short dashed contour identifies the integrated colors of LSB galaxies and the continuous contour limits the integrated colors of barred galaxies with outer rings. The arrow, in the lower right corner, indicates the reddening vector for galactic dust and the screen model approximation.

Furthermore, in the optical bands, the central galaxy is on average redder than the ringed barred galaxies. The inner regions of the ring are much bluer than the central galaxy, as already found for the colors of the non-scaled optical images (see previous section). In the NIR, on the contrary, the central galaxy and ring have similar colors. Since the ring component is very faint in these bands (as also suggested by the constant values of the colors in the last three areas, see Table 4) the corresponding colors may be influenced by background noise.

How do the NIR colors of ESO 235-G58 compare with typical colors of Polar Ring Galaxies? A common characteristic of ESO 235-G58 and PRGs is the very red nucleus with respect to the outer regions (see Fig. 12). The central galaxy of ESO 235-G58 has redder colors than the average PRG host galaxy (Iodice et al. 2002b,c).

7. Age estimate in ESO 235-G58

We wish to derive an estimate of the stellar population ages in the central galaxy and in the apparent inner pseudo-ring ring for this peculiar object and to compare them with the typical ages for other morphological galaxy types. To this aim, the stellar population synthesis model developed by Bruzual & Charlot (1993), GISSEL (*Galaxies Isochrone Synthesis Spectral Evolution Library*), was used to reproduce the $B-H$ and $J-K$ integrated colors of different regions (see Sect. 6) in ESO 235-G58. This wavelength range was already adopted by Iodice et al. (2002c) to estimate the age of the stellar populations in PRGs, since it helped in breaking the age-metallicity degeneracy (see also Bothun et al. 1984).

The GISSEL key input parameters are the Initial Mass Function (IMF), the Star Formation Rate (*SFR*), and the metallicity. In what follows, we have assumed that stars form according to the Salpeter (1955) IMF, in the range from 0.1 to 125 $M_\odot$.

In the NIR, where the perturbations due to dust are less significant, the morphology and colors of the central galaxy in ESO 235-G58, are very similar to a spiral galaxy (like an

Table 4. Integrated magnitudes and colors of different regions in ESO 235-G58. In the second column are listed the largest distances from the center (in arcsec) reached by each polygon.

Region	a (arcsec)	m_B (mag)	m_J (mag)	$B-V$	$V-I$	$B-H$	$J-K$	$J-H$	$H-K$
A1	2.7	18.51	14.72	1.18	1.65	4.78	1.36	0.99	0.36
A2	10	16.85	13.59	1.08	1.45	4.16	1.19	0.90	0.29
A3	18.2	16.22	13.23	0.99	1.36	3.84	1.12	0.85	0.26
A4	22.7	16.01	13.13	0.95	1.32	3.72	1.10	0.84	0.26
A5	40	15.7	13.05	0.85	1.24	3.49	1.10	0.84	0.26
RING		17.19	15.97	0.48	0.78	2.06	1.16	0.84	0.32

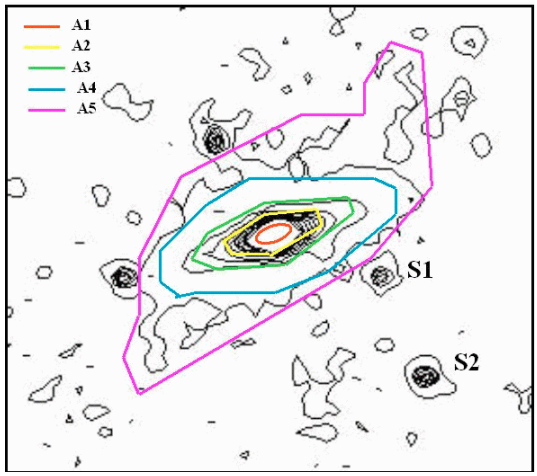

Fig. 11. ESO 235-G58 contour plot in Kn band (continuous line) plus the concentric five polygons limiting the areas where the integrated magnitudes are computed. The distance between the two stars (S1 and S2) is about 20″. North is at the top and East is to the left.

Sa galaxy), as emphasized in Sects. 3 and 6.2. Thus, for this component, we adopt a star formation history with an exponentially decreasing rate, $SFR(t) = \frac{1}{\tau}\exp(-t/\tau)$, with a very small time-scale τ, in order to approximate a single burst of star formation. The adopted values for the time scale parameter is $\tau = 1$ Gyr. The evolutionary tracks corresponding to this model were derived for different metallicities, which were assumed constant with age, and they are plotted in Fig. 13, for the $B-H$ and $J-K$ colors. The lines of constant age were computed from the evolutionary tracks: for the central galaxy in ESO 235-G58, they suggest an age between 1 to 3 Gyr. At this epoch, we derive a mass-to-light ratio for this component of $M/L = 1.3$.

As stressed in Sect. 3, the ring structure is too faint in the NIR bands to derive a realistic age estimate for this component, by using the $B-H$ and $J-K$ colors. Thus we used only optical colors ($B-V$ vs. $V-I$) to derive a characteristic age for the brightest stellar population. For this component, a constant star formation rate was adopted: this choice was mainly suggested by the active star formation regions observed in the B and V bands (see Fig. 1 and Buta & Crocker 1993). The ring structure seems to be much younger than the central galaxy: the last episode of star formation is recent and it may be not older than 10^8 yr. The mass-to-light ratio we estimate for this component at this age is $M/L = 0.04$.

The age for the central galaxy of ESO 235-G58 is very similar both to the typical age derived for the host galaxy in PRGs (see Iodice et al. 2002c) and for spiral galaxies; the ring component could be as young as the ring in NGC 4650A (Iodice et al. 2002a) and in ESO 603-G21 (Iodice et al. 2002c).

8. Study of the light distribution in the central galaxy of ESO 235-G58

In order to derive a quantitative morphology of ESO 235-G58 we performed a two-dimensional (2D) model of the central galaxy light distribution in the Kn band, where the perturbations by dust absorption are weaker. The 2D model we used to fit the surface brightness distribution in ESO 235-G58 is the same adopted to study the host galaxy light distribution in PRGs, which is described in Iodice et al. 2002b (see also Iodice et al. 2001). The Kn band light distribution in ESO 235-G58 was modeled by the superposition of a spheroidal central component, whose projected light follows the generalized de Vaucouleurs law, and an exponential disk. The structural parameters which characterized the light distribution of the spheroidal component are the *effective surface brightness* μ_e, the *effective radius* r_e, the *shape parameter* n and *apparent axial ratio* q_b; those relative to the disk are *the central surface brightness* μ_0, the *scalelength* r_h and *apparent axial ratio* q_d.

The regions affected by foreground stars and the ring light, which mainly perturbs the outer regions of the central galaxy along its major axis, are accurately masked, before the fit is performed. The structural parameters for bulge and disk components are listed in Table 5. The 2D model, for the central galaxy, in the J and H bands, and in the B, V, I bands, is a scaled version of the Kn band model, based on the average colors derived for this component (given in Table 4). The right panel of Fig. 14 shows the ratio between the whole image for ESO 235-G58 (i.e. including the outer ring) and the 2D model for the central galaxy, in the H band. The faint structures related to the ring are evident in this "residual image": these features are found around the central galaxy and they are elongated toward the NW and SE directions, at the edge of this component, along the major axis. In the regions corresponding to such features, in the Kn band, the galaxy is about 0.8 mag brighter than the model.

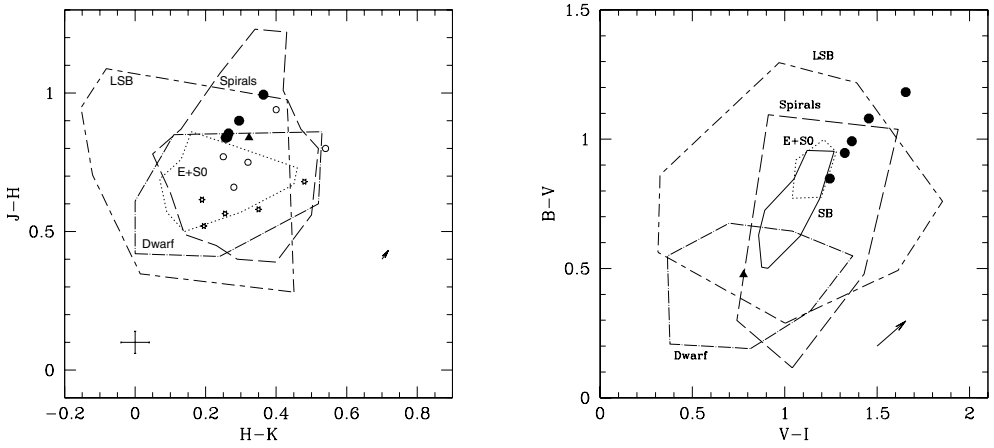

Fig. 12. $J-H$ vs. $H-K$ (*left panel*) and $B-V$ vs. $V-I$ (*right panel*) color diagram for the central galaxy (filled circles) and ring (filled triangles) in ESO 235-G58. Open circle indicates the colors of the nuclear regions in PRGs, and open stars indicate the average colors of the host galaxy in PRGs (data are from Iodice et al. 2002b,c). The dotted contour limits the region where the integrated colors of Es and S0s are found; the long-dashed contour limits the integrated colors of spirals; the dashed-dotted contour identifies the integrated colors of the dwarf galaxies and the long dashed–short dashed contour identifies the integrated colors of LSB galaxies and the continuous contour limits the integrated colors of barred galaxies with outer rings. The arrow, in the lower right corner, indicates the reddening vector for galactic dust and the screen model approximation.

Table 5. Structural parameters for the central galaxy, in the Kn band, for ESO 235-G58. The effective surface brightness μ_e and the central surface brightness μ_0 are in mag arcsec^{-2}, and μ_0^c is corrected for the inclination. r_e and r_h are respectively the effective radius and disk scalelength derived in arcsec, the corresponding values expressed in kpc are derived by using $H_0 = 70$ km s^{-1} Mpc^{-1}.

Parameter	Value
μ_e	15.52 ± 0.08
r_e (arcsec)	1.84 ± 0.08
r_e (kpc)	0.54 ± 0.02
μ_0	15.00 ± 0.03
μ_0^c	16.56 ± 0.05
r_h (arcsec)	4.71 ± 0.06
r_h (kpc)	1.39 ± 0.02
q_b	0.88 ± 0.02
q_d	0.237 ± 0.004
n	0.95 ± 0.08
B/D	0.7 ± 0.2
$\tilde{\chi^2}$	1.1

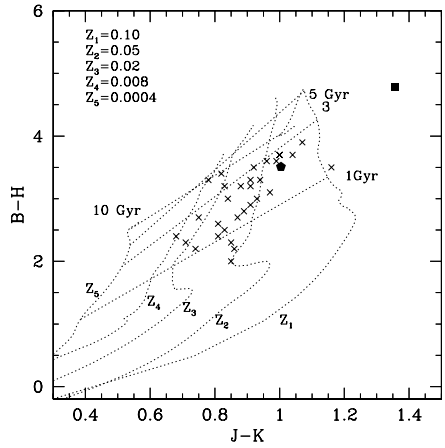

Fig. 13. $B-H$ vs. $J-K$ diagram of the evolutionary tracks for the stellar synthesis models optimized for the central galaxy in ESO 235-G58. The heavier dotted lines correspond to models with a characteristic timescale $\tau = 1$ Gyr. Models are computed for different metallicities as shown on this figure. Light dotted lines indicate loci of constant age for the different models; different ages are reported on the plot. The filled square and pentagon correspond respectively to the nucleus and the outer regions of the central galaxy in ESO 235-G58; crosses are for a sample of spiral galaxies (Bothun et al. 1984).

The comparison between the observed and calculated light profiles is shown in the left panel of Fig. 14: the light profiles along the major axis deviate from the exponential decrease in the range $10'' \leq R \leq 20''$, where the galaxy is about 0.6 to 0.8 mag brighter than the model. The analysis performed on the PA, ellipticity and surface brightness profiles, described in Sect. 4, lead us to conclude that the ring light adds on to the central component in this region. The excess of light, measured on the residual image, is comparable to those observed along the major axis light profiles between $10''$ and $20''$.

Along the minor axis, in the SW direction, the light distribution derived by the fit is brighter than the galaxy light ($\Delta\mu \leq 0.4$ mag), whereas, along the NE directions the galaxy light is more luminous than the model ($\Delta\mu \leq 0.4$ mag). These differences confirm the asymmetry of the minor axis profile, probably due to twisted isophotes in the inner regions ($R < 5''$), as already mentioned in Sects. 3 and 5.

By comparing the structural parameters which characterize the light distribution of the central galaxy in ESO 235-G58 with the typical values for different morphological types of galaxies, including PRGs (by Iodice et al. 2002a,b,c), we found that this component shows intermediate properties between PRGs and spiral galaxies. The Bulge-to-Disk (B/D) ratio obtained for ESO 235-G58 ($B/D = 0.7$), shown in Fig. 15 (left panel),

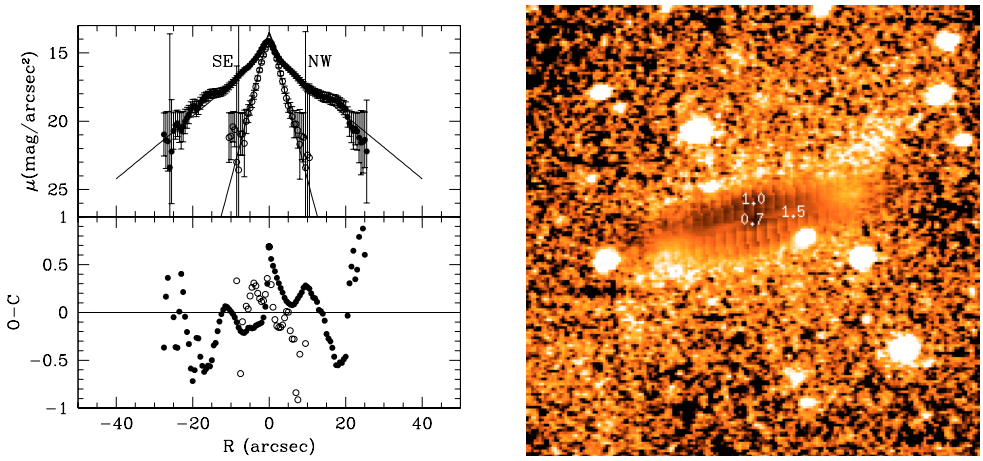

Fig. 14. *Left panel*: 2D fit of the K-band central galaxy light distribution in ESO 235-G58. The observed light profiles along the major (filled dots), PA = 106°, and minor axis (open dots), PA = 196°, are compared with those derived by the fit (continuous line), which was performed in the Kn band. The orientation, reported on the plot, refers to the major axis. *Right panel*: residual image obtained as the ratio between the whole image of ESO 235-G58 and the 2D model for the central galaxy in the H band. Units are intensity; whiter colors correspond to those regions where the galaxy is brighter than the model, darker colors correspond to those regions where the galaxy is fainter than the model. Numbers indicate the value of the ratio at that particular isophote. North is up and East is to the left.

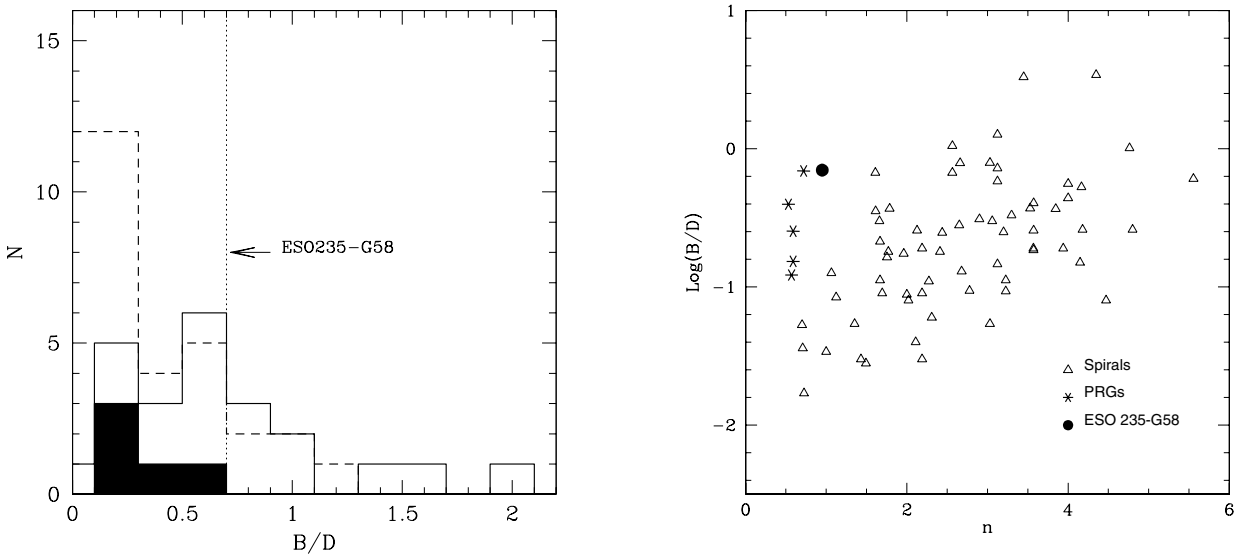

Fig. 15. B/D distribution for the PRGs (filled region), by Iodice et al. (2002b), for early-type galaxies (continuous line), by Bothun & Gregg (1990), and for spiral galaxies (dashed line), by Möllenhoff & Heidt (2001); Khosroshahi et al. (2000). The dotted line indicates the value of B/D derived for ESO 235-G58 (Table 5).

falls in the range of values typical for disk-dominated S0 galaxies and for spiral galaxies; furthermore it is also comparable with disk-dominated host galaxies in PRGs, such as ESO 415-G26 (see Iodice et al. 2002b). The right panel of Fig. 15 shows the correlation between the B/D ratio and the n exponent. The host galaxy of ESO 235-G58 is characterized by a higher value of the B/D ratio with respect to spiral galaxies, for the same value of n, as it is observed on average for PRGs. This is an effect caused by the differences in the disk scalelengths: the disks in ESO 235-G58 and in the PRG host galaxies ($\langle r_h \rangle = 0.9 \pm 0.5$ kpc) are smaller than disks observed in spiral galaxies ($\langle r_h \rangle = 4.5 \pm 2$ kpc, by Möllenhoff & Heidt 2001).

9. Study of ring light distribution in the *B* band

As pointed out in Sect. 3, the apparent inner pseudo-ring in ESO 235-G58, which surrounds the central galaxy, is very bright in the B and V bands, but it becomes quite faint in the NIR bands. Furthermore, it was also stressed that from the ring edges emerge two asymmetric spiral arms (Fig. 1). Thus, we studied the ring light distribution in the B band, where this component is brighter. The folded light profile in the B band was derived from surface brightness profiles extracted along the ring major axis in the two main directions (Sect. 4, Fig. 5). By fitting the ring light distribution with an exponential law, we derived an estimate of the central surface brightness, $\mu_0 = 25.80 \pm 0.05$ mag/arcsec^2, and of the scalelength,

$r_h = 23.0 \pm 0.5$ arcsec; $r_h = 6.7 \pm 0.2$ kpc. The scalelength of the ring structure in ESO 235-G58 is, on average, larger than the typical values for LSB galaxies, which are characterized by a mean value $r_h \sim 2 \pm 1$ kpc, in the range $0.15 \leq r_h(\mathrm{kpc}) \leq 9.26$ (by O'Neil et al. 1997); whereas it is comparable with the average value observed for spiral galaxies, $r_h \sim 6 \pm 3$ kpc ($0.83 \leq r_h(\mathrm{kpc}) \leq 23.5$, by de Jong 1996). This component is less extended than the polar structure in NGC 4650A, which has a typical scalelength of 8 kpc in the B band (Iodice et al. 2002a).

The ring surface brightness distribution $\mu(r)$ was used to derive the $\Delta R/\bar{R}$ ratio, where

$$(\Delta R)^2 = \frac{\int_{r_{\min}}^{\infty} (r - \bar{R})^2 \mu(r) \mathrm{d}r}{\int_{r_{\min}}^{\infty} \mu(r) \mathrm{d}r} \quad (1)$$

and $\bar{R}$ is the average radius, weighted by the surface brightness distribution, given by

$$\bar{R} = \frac{\int_{r_{\min}}^{\infty} r\mu(r) \mathrm{d}r}{\int_{r_{\min}}^{\infty} \mu(r) \mathrm{d}r} \quad (2)$$

and $r_{\min}$ is equal to 3 times the effective radius of the central component, in order to exclude the contribution from the central galaxy light. $\Delta R/\bar{R}$ is a key parameter in studies of polar ring stability (see Iodice et al. 2002a,c).

For the ring component in ESO 235-G58, $\Delta R/\bar{R} = 45\%$. This value is close to the lower limit in the range of values derived for a sample of spiral galaxies (de Jong 1996), which is $45\% \leq \Delta R/\bar{R} \leq 75\%$. On the other hand, it is near to the upper limit in the range of values derived for PRGs, which is $16\% \leq \Delta R/\bar{R} \leq 50\%$ (see Iodice et al. 2002a,c): it is comparable to the $\Delta R/\bar{R}$ ratio derived for the wide polar ring galaxies A0136-0801 (~45%) and NGC 4650A (~50%).

10. Discussion and conclusions

We have discussed the NIR and optical properties of the peculiar galaxy ESO 235-G58: an accurate photometric study in the optical bands led Buta & Crocker (1993) to classify ESO 235-G58 as an interacting system related to the polar ring galaxies. For this peculiar object, we have analyzed the light and color distribution in the NIR and optical bands and we have compared them with the typical properties observed for other morphological galaxy types, including polar ring galaxies (described in Iodice et al. 2002a,b,c). The main results of this analysis are the following:

1. the PA and ellipticity profiles are quite different from those observed for nearly face-on barred galaxies, but they are, on the other hand, very similar to the typical PA and ellipticity profiles observed for edge-on disk galaxies;
2. the high-frequency residual images confirm that the central galaxy in ESO 235-G58 has an edge-on disk;
3. the analysis of the color and light distribution in the central component strongly suggests that ESO 235-G58 is not a nearly face-on barred galaxy and that it shows many similarities to edge-on spiral galaxies and to the host galaxy in PRGs;
4. the outer ring structure is almost undetectable in the NIR bands: it is characterized by very blue colors which are similar to those of dwarf irregular galaxies and polar rings;
5. the central galaxy in ESO 235-G58 last formed a significant number of stars between 1 to 3 Gyrs ago, very similar both to the host galaxy in PRGs and for spiral galaxies. The last episode of stellar burst in the ring structure may be as recent as 10^8 yr, since its colors are comparable to those of the polar component in NGC 4650A and ESO 603-G21.

Furthermore, this peculiar galaxy is characterized by a high amount of neutral hydrogen, mainly associated with the ring component, as is also usually observed in many PRGs (van Gorkom et al. 1987; Arnaboldi et al. 1997; van Driel et al. 2000, 2002): the total HI mass is about 3×10^9 $M_\odot$ (Buta & Crocker 1993; van Driel et al. 2000, 2002). We derive a total mass for the stellar component of about 4×10^7 $M_\odot$, assuming a mass-to-light ratio $M/L = 0.04$ (see Sect. 7). The total mass for the stellar component of the central galaxy is about 2.1×10^9 $M_\odot$, assuming $M/L = 1.3$ (see Sect. 7). The total *baryonic mass* in the ring structure, i.e. stellar plus gaseous component, is then about 1.4 times larger than the total mass of the stellar component in the central galaxy. A value larger than unity for the *total baryonic mass*-to-*stellar mass* ratio is commonly observed for PRGs (see Iodice et al. 2002a,c).

The low inclination angle between the central galaxy and ring (40°, by Buta & Crocker 1993), which is unusual in PRGs, may suggest that the interaction is recent and the ring may not yet have reached a stable configuration or it may be a transient structure. Connecting ESO235-G58 to PRGs is important to know this. The ring's low inclination with respect to the equatorial plane of the central galaxy makes ESO 235-G58 very similar to another *polar-ring-related* object, NGC 660 (van Driel et al. 1995). According to the latest N-body simulations by Bournaud & Combes (2003), such objects are likely to be formed through an accretion mechanism, where gas is accreted by the host galaxy from a gas-rich donor. Bournaud & Combes' scenario can account for both nearly polar structures, and more shallowly-inclined rings, whose radial extension $\Delta R/\bar{R}$ can be up to 55%. These predictions are consistent with the observed values for these parameters in ESO 235-G58 (see Sects. 1 and 9).

The stability of such inclined structures depends on the ring mass and the dark matter distribution; for a ring at low inclination with respect to the equatorial plane whose mass is 30% of the visible total mass in the system, those numerical simulations (Bournaud & Combes 2003, see Sect. 6.3) predict that the ring is unstable, but will not disrupt within a timescale of 2.5 Gyrs in a nearly spherical dark halo. In the case of ESO 235-G58, the ring mass (stars plus gas) is about 60% of the visible total mass in the system, and information on the dark halo shape can be derived from the position of ESO 235-G58 in the $L_B - \mathrm{Log}(W_{20})$ plane (where L_B is the total luminosity of the whole system), as described by Iodice et al. (2003). The L_B, $\mathrm{Log}(W_{20})$ values for ESO 235-G58 fall on the average Tully-Fisher relation for bright disk galaxies (see Iodice et al. 2003, Fig. 2): this implies that the dark halo in ESO 235-G58

may be nearly spherical. Thus the ring will probably persist for still longer than 2.5 Gyrs.

The present work leads us to conclude that ESO 235-G58 is a *polar-ring-related* galaxy, characterized by a low inclined ring/disk structure. Such inclined structures are rarely observed, because they are less stable than those nearly polar and they can be easily confused with barred galaxies, as it seems to have happened in the case of ESO 235-G58. This peculiar galaxy provides us with an intriguing face-on view of the low-inclined disk component of a PRG-related object. Kinematic observations are urgently needed to further understand the structure of this enigmatic object. The analysis of high resolution observations would provide further insights into the effects of the interaction on both the inner component and the inclined disk.

Acknowledgements. The authors would like to thank the anonymous referee whose comments and suggestions let us improve the presentation of this work. E.I. would like to thank G. De Lucia for the help in the use of GISSEL. The authors wish to thank the Mt. Stromlo and Siding Spring Observatories for the observing time at the 2.3 m telescope allocated to this project. R.B. acknowledges the support of NSF grant AST-0205143 to the University of Alabama and LSS acknowledges support from AST-0139563.

References

Arnaboldi, M., Freeman, K. C., Sackett, P. D., Sparke, L. S., & Capaccioli, M. 1995, Planetary Space Sci., 43, 1377
Arnaboldi, M., Oosterloo, T., Combes, F., Freeman, K. C., & Koribalski, B. 1997, AJ, 113, 585
Athanassoula, E., Morin, S., Wozniak, H., et al. 1990, MNRAS, 245, 130
Bell, E. F., Banaby, D., Bower, R. G., et al. 2000, MNRAS, 312, 470
Bothun, G. D., & Gregg, M. D. 1990, ApJ, 350, 73
Bothun, G. D., Romanishin, W., Strom, S. E., & Strom, K. M. 1984, AJ, 89, 1300
Bournaud, F., & Combes, F. 2003, A&A, 401, 817
Bruzual, G., & Charlot, S. 1993, ApJ, 405, 538
Buta, R., & Crocker, D. A. 1992, AJ, 103, 1804
Buta, R., & Crocker, D. A. 1993, AJ, 106, 939
Buta, R. 1995, ApJS, 96, 39
Cardelli, J. A., Clayton, G. C., & Mathis, J. S. 1989, ApJ, 345, 245
de Jong, R. S. 1996, A&AS, 118, 557
de Jong, R. S., & van der Kruit, P. C. 1994, A&AS, 106, 451
de Vaucouleurs, G., de Vaucouleurs, A., Corwin, H. G., et al. 1991, Third Reference Catalog of Bright Galaxies (Springer) (RC3)
Erwin, P., & Sparke, L. S. 2003, ApJS, 146, 299
Iodice, E., D'Onofrio, M., & Capaccioli, M. 2001, Ap&SS, 276, 869
Iodice, E., Arnaboldi, M., De Lucia, G., et al. 2002a, AJ, 123, 195
Iodice, E., Arnaboldi, M., Sparke, L. S., Gallagher, J. S., & Freeman, K. C. 2002b, A&A, 391, 103
Iodice, E., Arnaboldi, M., Sparke, L. S., & Freeman, K. C. 2002c, A&A, 391, 117
Iodice, E., Arnaboldi, M., Bournaud, F., et al. 2003, ApJ, 585, 730
Jungwiert, B., Combes, F., & Axon, D. J. 1997, A&AS, 125, 479
Khosroshahi, H. G., Wadadekar, Y., & Kembhavi, A. 2000, ApJ, 533, 162
Knapen, J. H., Hes, R., Beckman, J. E., & Peletier, R. F. 1991, A&A, 241, 42
Makarova, L. 1999, A&AS, 139, 491
McGaugh, S. S., Schombert, J. M., Bothun, G. D., & de Blok, W. J. G. 2000, ApJ, 533, 99
McGregor, P. J. 1994, PASP, 106, 508
Michard, M. 1984, A&A, 140, 139
Michard, R., & Poulain, P. 2000, A&AS, 137, 245
Möllenhoff, C., & Heidt, J. 2000, A&A, 368, 16
O'Neil, K., Bothun, G. D., Schombert, J., Cornell, M. E., & Impey, C. D. 1997, AJ, 114, 2448
Reshetnikov, V. P., Faundez-Abans, M., & de Oliveira-Abans, M. 2002, A&A, 383, 390
Rieke, G. H., & Lebofsky, M. J. 1985, ApJ, 288, 618
Salpeter, E. E. 1955, ApJ, 121, 161
Schlegel, D. J., Finkbeiner, D. P., & Davis, M. 1998, ApJ, 500, 525
Scorza, C., & Bender, R. 1995, A&A, 293, 20
van Driel, W., Combes, F., Casoli, F., et al. 1995, AJ, 109, 942
van Driel, W., Arnaboldi, M., Combes, F., & Sparke, L. S. 2000, A&AS, 141, 385
van Driel, W., Combes, F., Arnaboldi, M., & Sparke, L. S. 2002a, A&A, 386, 140
van Gorkom, J. H., Schechter, P. L., & Kristian, J. 1987, ApJ, 314, 457
Walterbos, R. A. M., & Kennicutt, Jr. R. C. 1988, A&A, 198, 61
Whitmore, B. C., Lucas, R. A., McElroy, D. B., et al. 1990, AJ, 100, 1489
Wozniak, H., Friedli, D., Martinet, L., Martin, P., & Bratschi, P. 1995, A&AS, 111, 115